Microchemical Journal 181 (2022) 107678

Contents lists available at ScienceDirect

Microchemical Journal

journal homepage: www.elsevier.com/locate/microc

Considerations on the use of spectroelectrochemistry in reflection mode for quantitative analysis: Study of the Fe(III)/Fe(II) – orthophenanthroline system

G. Sirin Ustabasi [a], Julio Bastos-Arrieta [b,c], Clara Pérez-Ràfols [b,c], Núria Serrano [b,c], José Manuel Díaz-Cruz [b,c,*]

[a] Department of Chemistry, Faculty of Science and Letters, Istanbul Technical University, Maslak, Istanbul 34469, Turkey
[b] Departament d'Enginyeria Química i Química Analítica, Universitat de Barcelona (UB), Martí i Franquès 1-11, E08028 Barcelona, Spain
[c] Institut de Recerca de l'Aigua (IdRA), Universitat de Barcelona (UB), 08028 Barcelona, Spain

ARTICLE INFO

Keywords:
Spectroelectrochemistry
Screen-printed electrodes
Iron-orthophenanthroline complexes
Cyclic voltammetry
Chronoamperometry
Chronoabsorptometry
Iron(III) determination

ABSTRACT

Theoretical and experimental considerations are made about possible analytical applications of spectroelectrochemistry (SEC) in reflection mode using screen-printed electrodes. The system Fe(III)/Fe(II) – orthophenanthroline is taken as a model of electrochemical generation and consumption of a substance that is strongly absorbing: the Fe(II) – orthophenanthroline complex. Different possibilities of quantification are discussed, including cathodic and anodic peaks in cyclic voltammetry and both electrochemical and optical signals acquired in chronoamperometric experiments. Among these, the evolution of absorbance with the square root of time at a constant potential has shown interesting possibilities for the determination of Fe(III)-ion at micromolar level (LOD = 2 10^{-6} mol L^{-1}). Moreover, this method appears to be resistant to the presence of other electroactive species such as Cu(II)-ions.

1. Introduction

Spectroelectrochemistry (SEC) is a hybrid technique arising from the combination of simultaneous electrochemical and spectroscopic measurements focused on substances electrochemically and optically active [1–4]. Since it was introduced in 1964 by Kuwana et *al.* [5], SEC has been mainly used in the study of mechanisms of electrochemical reactions and for the characterisation of materials, but scarcely for quantitative analysis [4,6]. Among the different spectral ranges used, UV/vis and NIR are the most popular and, depending on the instrumental configuration, absorption, reflectance, fluorescence or Raman spectra can be acquired [6].

For many years, SEC measurements were restricted to optically transparent electrodes [1–4], but the use of thin-layer long-pathway spectroelectrochemical cells [7] and some reflection setups [8,9] allowed the use of non-transparent electrodes such as carbon paste or glassy carbon electrodes, and even bismuth-film electrodes [10]. Recently, the increasing use of commercial screen-printed electrodes (SPE) as a simple to handle and modify, cost-effective, reproducible and versatile alternative to conventional solid electrodes [11–14] has provided a valuable tool to reinforce the possibilities of SEC for analytical purposes. In this context, the pioneering work of the group of Heras, Colina and López-Palacios is remarkable. They designed a device to carry out reflection SEC measurements (normal configuration) in the UV/vis region using SPE units. This experimental setup was successfully applied to the determination of dopamine and to the study of its oxidation mechanism [15] and it is, indeed, the precursor of the commercial reflection equipment used in the present study. The same group has made important progress in the application of SEC measurements in parallel configuration based on bare optical fibres [16–19]. This approach has proved to be more sensitive than the normal configuration and, hence, more appropriate for the determination of analytes. However, to the best of our knowledge, no commercial equipment is yet available with this configuration, which significantly hinders its implementation as a routine analytical technique.

Thus, in this work, we investigate as a proof of concept the suitability of SEC in reflection mode for quantitative analysis. For this purpose, we have chosen the Fe(II)/Fe(III) system in the presence of 1,10-phenanthroline, also known as ortho-phenanthroline (OP), as a model. OP is a well-known ligand used for the spectrophotometric determination of

* Corresponding author.
E-mail address: josemanuel.diaz@ub.edu (J.M. Díaz-Cruz).

https://doi.org/10.1016/j.microc.2022.107678
Received 3 April 2022; Received in revised form 8 June 2022; Accepted 9 June 2022
Available online 11 June 2022

Fe(II) in the visible region, since a strongly coloured $Fe(OP)_3^{2+}$ complex is formed with quite high stability constants. If we consider the overall stability constants of the successive ML_n complexes in the form $\beta_n = [ML_n]/([M][L]^n)$, the logarithms of such constants are: $\log \beta_1 = 5.85$, $\log \beta_2 = 11.15$, $\log \beta_3 = 21.0$ [20]. As for the absorption capabilities, recent experiments have determined a molar absorptivity of $\varepsilon = 12450\ mol^{-1}\ L\ cm^{-1}$ at 510 nm [21]. Concerning to Fe(III), it also forms OP complexes, but with lower stability ($\log \beta_1 = 6.5$, $\log \beta_2 = 11.4$, $\log \beta_3 = 14.1$, also extracted from [20]) and much lower absorptivity. These features are very promising for the SEC analysis of Fe(III)-ion in the presence of OP, since its progressive reduction to Fe(II) generates a strongly coloured complex that can be optically detected. In fact, the use of OP has provided excellent results in the stripping voltammetric analysis of Fe(III) using a carbon SPE [22]. In this work, Cu(II)-ions were also analysed, since they form stable and electroactive complexes with OP ($\log \beta_1 = 9.08$, $\log \beta_2 = 15.8$, $\log \beta_3 = 21.0$, according to [20]). and could be a valuable model of interference in the detection of Fe(III).

A key point in the design of a quantitative analytical method is the improvement of the signal-to-noise ratio. To achieve this, the optical data acquired at 2007 wavelengths by SPELEC detector have been compressed by means of a discrete wavelet transform (DWT), a strategy that provided good results in a previous work with this kind of spectra [23]. Another important point is the selection of the most convenient equations to fit to experimental data. This is why the introduction is followed by a theoretical section with an overview of the expressions, mostly coming from transmission cells with optically transparent electrodes that could be applicable to the reflection case [1–3].

2. Theory

In normal configuration (Fig. 1), a reflection probe is used, which includes a central optical fiber surrounded by six additional fibres. The external fibres uniformly illuminate a reduced region of the electrode surface with all the wavelengths coming from the radiation source, and the central fiber captures a part of the radiation reflected by the surface (coming from a surface even more reduced). Such captured radiation is analysed by a diode array detector and the light intensity at every wavelength is quantified in counts.

Let us consider the geometry described by Fig. 1, where R_1 is the radius of the working electrode of the SPCE unit, R_2 is the radius of the reflected light beam collected by the central fiber, d is the distance between the probe and the electrode surface (a few mm) and δ is the width of the diffusion layer (a few μm). If the drops of the solution are properly inserted in the reflection cell, all the space between the probe and the electrode is filled with solution.

In the test solutions employed in this work, there is a bulk concentration of Fe(III)-ion and an excess of the ligand OP, which ensures that all the metal is in the complexed form $Fe(OP)_3^{3+}$. At the electrode surface, the complex is reduced to the form $Fe(OP)_3^{2+}$, whose colour is much more intense than that of the oxidised complex (especially at 510 nm):

$$Fe(OP)_3^{3+} + 1e^- \rightarrow Fe(OP)_3^{2+} \quad (1)$$

In the beginning of the measurement, the bulk concentration of the oxidised complex is c^*_{ox}, that is, the concentration of Fe(III) in the test solution, whereas the bulk concentration of the reduced complex is $c^*_{red} = 0$. If we apply a constant potential negative enough to reduce the Fe (III) complex at the maximum rate (i.e., controlled by diffusion), the Cottrell Equation for a planar electrode holds [3]:

$$I = \frac{nFSD^{1/2}c^*_{ox}}{\pi^{1/2}t^{1/2}} \quad (2)$$

where I is the electrical current, n is the number of electrons involved in the redox process (1 in this case), F is the Faraday constant, D is the

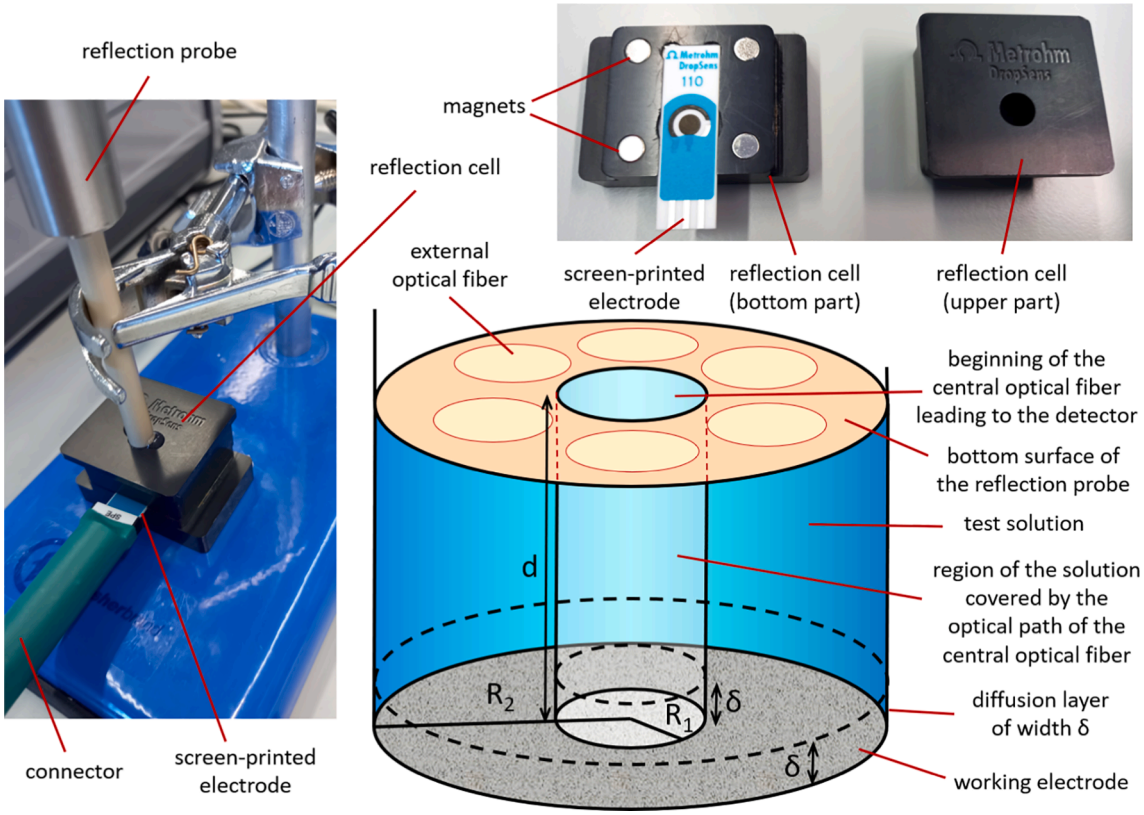

Fig. 1. Scheme of the reflection cell setup used in this work, showing the space comprised between the optical probe and the screen-printed unit. The sizes of the central and the six external optical fibres and the diffusion layer have been redimensioned, so that in practise $R_1 \ll R_2$ and $\delta \ll d$. The light entering the central fiber comes from the reflection of the light provided by the optical fibres surrounding the central one, which cover a radius quite bigger than R_1.

diffusion coefficient of the oxidised complex (similar to that of the reduced complex), t is the time and S is the electrode surface (πR_2^2 in our case). It is worth noting that, although in electrochemistry the electrode surface is usually denoted by A, in this work we will use S to prevent confusion with the optical absorbance.

If we divide the current by nFS we get the flux J, i.e., the number of mols of $Fe(OP)_3^{3+}$ that are consumed at the electrode per unit of time and surface. Taking into account Eqn. (1), J is also the number of mols of $Fe(OP)_3^{2+}$ that are produced at the electrode per unit of time and surface:

$$J = \frac{I}{nFS} = \frac{D^{1/2}c_{ox}^*}{\pi^{1/2}t^{1/2}} \tag{3}$$

Now, let us consider the absorbance A measured in the reflection cell at a fixed wavelength where only the reduced complex absorbs. According to the Beer's Law for the optical path shown in Fig. 1:

$$A = \log_{10}\frac{P_0}{P} = \varepsilon c_{red} d \tag{4}$$

where P and P_0 are the radiant power (or light intensity) measured in the sample and in the reference, respectively, d is the optical path (in practice, the distance between the probe and the electrode), and ε and c_{red} are the molar absorptivity and the concentration of the reduced complex inside the optical path, respectively. In SPELEC, P is measured in counts and the reference can be a blank solution including only the supporting electrolyte or the same sample just before starting the SEC measurement.

As for c_{red}, Beer's law assumes a homogeneous distribution of the absorbing substance along the optical path and, obviously, this is not the case for the reduced complex, which is not initially present in the solution and is progressively generated at the electrode surface and diffusing towards the probe. Nevertheless, the reduced complex cannot go further the frontier delimited by the width of the diffusion layer δ, which is increasing with time but always will be much smaller than the optical path d. In a first approach, we can compute c_{red} as the number of mols of reduced complex (n_{red}) generated by the portion of the electrode surface covered by the detected beam divided by the volume of solution where the beam passes (V):

$$c_{red} = \frac{n_{red}}{V} = \frac{n_{red}}{\pi R_1^2 d} \tag{5}$$

The value of n_{red} for a given time t can be deduced from the flux J, multiplying it by the constant surface defined by the beam radius (πR_1^2) and integrating it with respect to time:

$$n_{red} = \int_o^t \pi R_1^2 J dt = \pi R_1^2 \int_o^t J dt \tag{6}$$

If we use Eqn. (3) for expressing the flux as a function of time and combine it with Eqn. (6), we get:

$$n_{red} = \pi R_1^2 \int_0^t \frac{D^{1/2}c_{ox}^*}{\pi^{1/2}} t^{-1/2} dt = \pi^{1/2} R_1^2 D^{1/2} c_{ox}^* \int_0^t t^{-1/2} dt = \tag{7}$$

$$= 2\pi^{1/2} R_1^2 D^{1/2} c_{ox}^* t^{1/2}$$

Then, using Eqn. (5), c_{red} is:

$$c_{red} = \frac{n_{red}}{\pi R_1^2 d} = \frac{2D^{1/2}c_{ox}^* t^{1/2}}{\pi^{1/2} d} \tag{8}$$

and, substituting in Eqn. (4), we obtain the following expression for the absorbance, which is the same holding for transmission SEC experiments [1–3]:

$$A = \frac{2D^{1/2}\varepsilon}{\pi^{1/2}} c_{ox}^* t^{1/2} \tag{9}$$

Equation (9) sets up a straightforward relationship among relevant parameters of the system and time. However, until now, it has been only used for measuring diffusion coefficients in long-pathway cells [1–3]. This expression states that the absorbance measured in reflectance mode does not depend on the distance between the electrode and the optical probe nor on the width of the beam covered by the central optical fiber attached to the detector. Moreover, it is directly proportional to the bulk concentration of the reagent (the oxidised complex in our case), the molar absorptivity of the coloured product (the reduced complex) and the square root of the time. This is especially useful in chronoamperometric (CA) measurements using a single potential step, were the planar nature of screen-printed electrodes ensures the fulfilment of the Cottrell Equation and were measurements provide a large deal of data as a function of time. Eqn. (9) predicts that in chronoamperometric SEC measurements the plots of absorbance versus $t^{1/2}$ should be linear with the following slope [1–3]:

$$slope(Avs.t^{1/2}) = \frac{2D^{1/2}\varepsilon}{\pi^{1/2}} c_{ox}^* \tag{10}$$

And, if the slopes obtained for different concentrations of the oxidised complex are plotted versus such concentration, a 'slope of slopes' should be obtained which only depends on the diffusion coefficient of both complexes and the molar absorptivity of the reduced complex (the coloured product of the electrochemical reaction):

$$slope(slopesvs.c_{ox}^*) = \frac{2D^{1/2}\varepsilon}{\pi^{1/2}} \tag{11}$$

This can be used to estimate the diffusion coefficient from the molar absorptivity or vice-versa.

Finally, taking the derivative of the absorbance with respect to the time and substitute the Cottrell Equation (2) in it:

$$\frac{dA(t)}{dt} = \frac{D^{1/2}\varepsilon}{\pi^{1/2}} c_{ox}^* t^{-1/2} = I(t)\frac{\varepsilon}{nFS} \tag{12}$$

Although this relationship is only true under diffusion-controlled conditions (typical of amperometry), it could be roughly extrapolated to the situation where both I and A simultaneously depend on potential and time, as it happens in cyclic voltammetry. This would justify that the derivative of the absorbance with respect to time has a similar shape of the corresponding cyclic voltammogram. The key factor deciding which signal is more sensitive is the term ε/nFS. This means that, as expected, optical measurements would benefit from high molar absorptivities and voltammetric measurements would be enhanced with large electrode surfaces. A very important question, however, is the role of the noise in both measurements, that could be determinant in the choice of the more convenient signal for analytical purposes. Such question will be stated again when discussing experimental data.

It is also interesting to consider the applicability of the previous equations when the coloured substance is not generated, but disappearing at the electrode surface. This would be the case of the oxidation of Fe(II) in the presence of an excess of OP when a constant oxidative potential is used (much more positive than this employed for the reduction of Fe(III)):

$$Fe(OP)_3^{2+} \rightarrow Fe(OP)_3^{3+} + 1\ e^- \tag{13}$$

This electrochemical process causes a decrease in the concentration of the reduced complex (with higher molar absorptivity than the oxidised one). If measurements are still carried out at the maximum of absorption of the reduced complex, there will be a decrease of the absorbance with time. Thus, using Eqn. (4) with the initial spectrum as a blank, we will get negative absorbances as the solution progressively loses its colour due to the oxidation of the reduced complex:

$$A = \log_{10}\frac{P_0}{P} = \varepsilon \Delta c_{red} d \tag{14}$$

where both the absorbance A and the variation of the concentration of the reduced species Δc_{red} are negative. Then, the concentration decrease

can be related to the flux of Eqn. (3), but now written in terms of c_{red}* (the initial bulk concentration of the reduced complex) instead of c_{ox}*. Thus, following an analogous development, we can achieve an expression equivalent to Eqn. (9) for the case of a constant potential producing the decrease of the concentration of the absorbing species and, hence, negative values of absorbance:

$$-A = \frac{2D^{1/2}\varepsilon}{\pi^{1/2}} c^*_{red} t^{1/2} \tag{15}$$

where ε is still the absorptivity at the optimal wavelength for the reduced complex and the negative absorbance is transformed into a positive number with the '-' sign.

Finally, it is interesting to consider that the equations above have been deduced considering that the current I is proportional to the geometrical area of the electrode $S = \pi R^2$. However, this is only true in mirror-like polished electrodes. In rough surfaces such as these of screen-printed electrodes the effective area S' contributing to the electrochemical process can be quite bigger that the geometrical one S. Then, the current is proportional to S' but the flux and the volume covered by the light beam have to be computed with S. If we define the rugosity coefficient f_R in the form:

$$f_R = S'/S \tag{16}$$

then, Eqns. (2) and (3) can be rewritten in the form:

$$I = \frac{nFS' D^{1/2} c^*_{ox}}{\pi^{1/2} t^{1/2}} = \frac{nFSf_R D^{1/2} c^*_{ox}}{\pi^{1/2} t^{1/2}} \tag{17}$$

$$J = \frac{I}{nFS} = \frac{D^{1/2} f_R c^*_{ox}}{\pi^{1/2} t^{1/2}} \tag{18}$$

and Eqn. (10) becomes:

$$slope(A vs. t^{1/2}) = \frac{2f_R D^{1/2}\varepsilon}{\pi^{1/2}} c^*_{ox} \tag{19}$$

which can be useful for an accurate determination of diffusion coefficients.

3. Material and methods

3.1. Chemicals

Analytical grade chemicals were utilized in all experiments. These chemicals were acquired from Merck (Darmstadt, Germany), except for orto-phenanthroline, which was purchased from J.T. Baker (Pennsylvania, USA). Stock solutions of Fe(III) and Cu(II) were prepared from their salts and standardized. Purified water (with electrical resistivity of 18.4 MΩ cm) was obtained from Milli-Q Reference A + Water Purification System (Millipore, France) to prepare all solutions. Finally, all of the prepared solutions were kept at +4 °C until their use.

3.2. Spectroelectrochemical measurements

Spectroelectrochemical (SEC) measurements were conducted with a SPELEC equipment from Metrohm DropSens (Oviedo, Spain) controlled by the DropView SPELEC software system (Version 3.2.2). All measurements were carried out in a SEC cell (ref. DRP-REFLECELL 70055) in normal configuration, i.e., with the screen-printed electrode and the optical probe placed horizontally and vertically, respectively.

Samples were inserted into the measuring device by first placing 50 μL of sample onto the working electrode of the screen-printed carbon electrode (SPCE) unit, fixed onto the lower part of the cell (Fig. 1). The cell was closed inserting the upper part, which remained fixed with a set of eight magnets. Then, an additional volume of 50 μL was added through the hole on the top of the cell. Presence of any air bubbles was checked and prevented prior to the measurement. Once the sample was placed in the cell, the optical probe was introduced slowly in the hole and some extra drops were allowed to spill out from the sides of the probe. The cell was thoroughly washed with water after each measurement and a fresh drop was used every time. Also, a new SPCE was used for each set of measurements. SPCE devices, with a 4 mm diameter working electrode, were provided by Metrohm DropSens (DRP-110, Spain) and connected by means of a flexible cable provided by Metrohm DropSens (ref. CAST).

Unless otherwise indicated, SEC measurements were conducted in solutions containing 25 mmol L^{-1} of OP in acetate buffer 0.1 mol L^{-1} (pH 4.5). Cyclic voltammetric (CV) measurements were scanned between −0.3 V and 1.1 V with a scan rate of 50 mV s^{-1}. Chronoamperometric (CA) measurements were carried out at a fixed potential of −0.4 V every 0.5 s during 90 s. Integration time was set to 1000 ms for all spectrometric measurements considering a wavelength range from 200 nm to 900 nm.

3.3. Data treatment

Raw experimental data were imported from DropView software to Excel® and Matlab® environments and processed with home-made programs written in Matlab language [24]. Raw optical spectra in counts acquired at 2007 wavelengths were submitted to four-level discrete wavelet transform (DWT) using Daubechies 4 function, which provided good results in the compression and denoising of spectra acquired with SPELEC in a previous study [23]. Absorbance spectra were computed from raw spectra or DWT-denoised spectra in counts using as a reference the corresponding spectra measured for the sample solution prior to the SEC measurement. In both cases, Eqn. (14) was applied to get the absorbance value for a given wavelength as $A = \log_{10}(p_0/p)$, were p_0, p are the counts measured before starting the electrochemical measurement and at the time when the absorbance is going to be computed, respectively. In practical terms, this means applying the equation above, element by element, to couples of vectors of 2007 or 258 points to get single absorbance vectors of 2007 or 258 points.

4. Results and discussion

4.1. Preliminary voltammetric study

CV was used for a preliminary study of the Fe(III)-OP system. Fig. 2 compares the CV signals obtained at different concentrations of both substances. Fig. 2a shows in red colour a CV of Fe(III) in the absence of OP. In the forward scan there is a reduction peak of Fe(III)-ion at *ca.* −0.2 mV, whereas in the backward scan there is a broad peak at *ca.* 0.2 V corresponding to the reoxidation of the Fe(II)-ion generated in the forward scan. The CV of OP alone, in blue colour, presents a significant capacitive current (large vertical distance between the currents in both scans as compared to the blank of the buffer) and several cathodic signals: one relatively small and very broad at *ca.* 0.2 mV and another very large starting at *ca.* −0.4 V. It is not clear whether these signals are due to the reduction of OP or to an enhanced reduction of the solvent. Anyway, the second signal restricts the working potential to values more positive than −0.4 V. Finally, the CV of a mixture of Fe(III) and OP, in green colour, shows a cathodic peak in the forward scan at *ca.* 0.2 V and an anodic peak in the backward scan at *ca.* 0.9 V. The cathodic peak can be undoubtedly assigned to the reduction of the oxidised form of the iron complex $(Fe(OP)_3^{3+})$ present in the solution. As for the anodic peak, it is due to the reoxidation of the reduced complex generated previously in the forward scan and which remains in the diffusion layer. If we compare both peaks with those obtained for the same concentration of Fe(III) in the absence of OP, we see that they are quite bigger, and much better shaped in the case of the anodic one. This fact suggests that the formation of OP complexes with Fe(II) and Fe(III) favours the electrochemical processes of this redox pair. Moreover, both peaks are

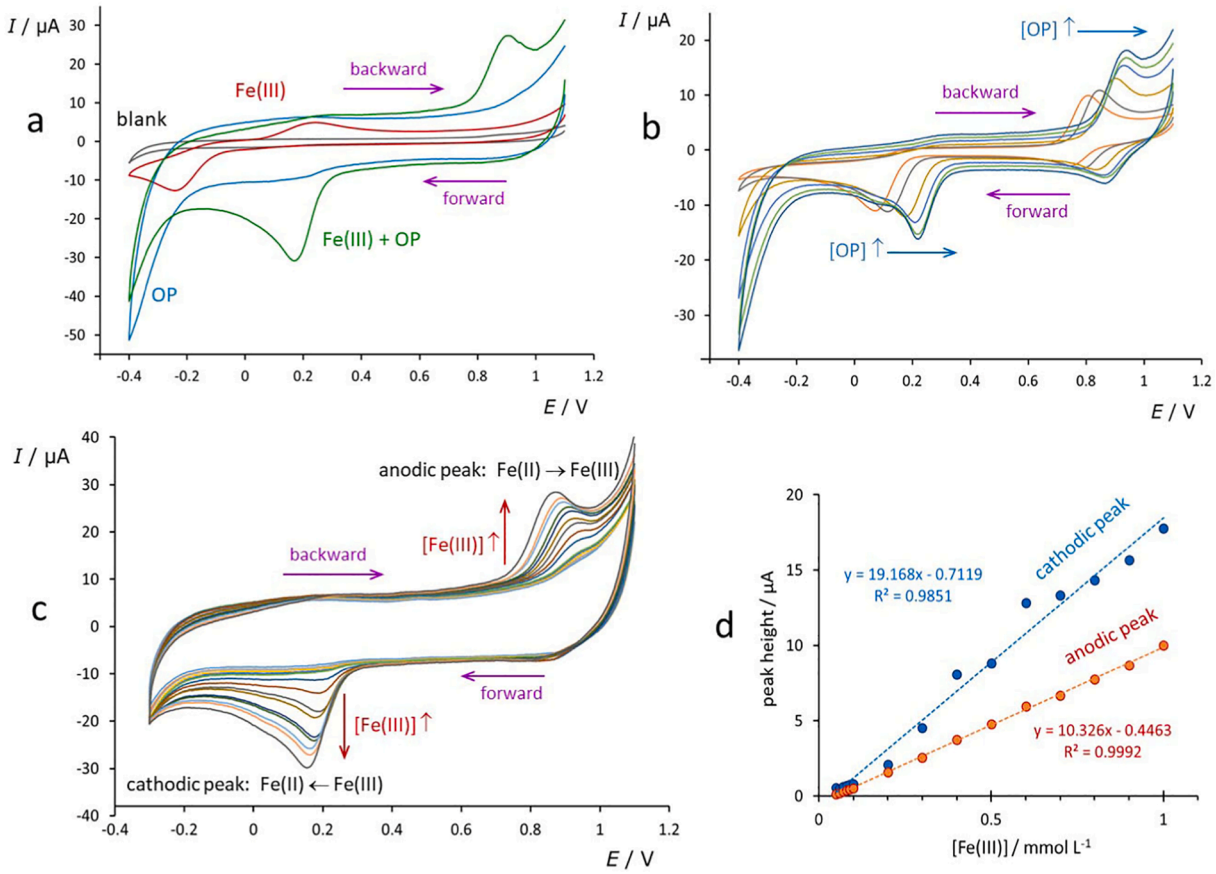

Fig. 2. Results of the preliminary CV study. a) CV signals obtained for the buffer alone, and solutions of Fe(III) 1.0 mmol L^{-1}, OP 25 mmol L^{-1}, and Fe(III) 1.0 mmol L^{-1} + OP 25 mmol L^{-1}; b) evolution of CV signals for a Fe(III) solution 1.0 mmol L^{-1} and concentrations of OP 5, 10, 25, 50, 75 and 100 mmol L^{-1}; c) evolution of CV signals for a OP solution 25 mmol L^{-1} and increasing concentrations of Fe(III) within the range 0.05 – 1.0 mmol L^{-1}; d) calibration plots obtained from the heights of cathodic and anodic peaks shown in c. The directions of the scans are denoted with purple arrows.

dramatically moved to more positive potentials (more than 0.4 V the cathodic peak and more than 0.7 V the anodic one). Fig. 2b shows that this shift is progressive as the concentration of OP increases. This can be explained considering that the 1:3 complex of OP with Fe(II) (predominant at large excess of OP) is quite more stable than the analogous complex of Fe(III), which stabilises the reduced species as compared to the oxidised one. Thus, it is not surprising that the addition of OP makes Fe(III) easier to be reduced (cathodic peak potential less negative) and Fe(II) more difficult to be oxidised (anodic peaks more positive). At the view of these results, an intermediate concentration of 25 mmol L^{-1} of OP was selected for further experiments, in order to assure enough excess of ligand and to prevent too large interfering cathodic signals.

Fig. 2c shows that, for a fixed concentration of OP 25 mmol L^{-1}, successive additions of Fe(III)-ion cause a progressive increase of both peaks, thus confirming that they are caused by the reduction and oxidation of Fe(III) and Fe(II) complexes, respectively. A slight negative shift of the potentials is also observed as the concentration of iron increases (in opposition to the trend shown in Fig. 2b at increasing concentrations of OP). Fig. 2d evidences a very good linear relationship between the anodic peak and the concentration of Fe(III), whereas linearity is not as good in the case of the cathodic peak, probably because of the interference of the cathodic signals of OP mentioned above.

An additional study was made by differential pulse voltammetry (DPV), a very popular technique for analytical purposes. As shown in Fig. S1, a reduction signal of the complex of Fe(III) appears at *ca.* 0.1 V, i.e., the same potential region as the cathodic signal in CV. However, the peak is quite distorted and noisy, probably due to the above-mentioned cathodic signals of OP. Moreover, there is not a linear dependence of the peak height with the concentration of Fe(III). Consequently, DPV was discarded for the further studies.

4.2. SEC study by means of cyclic voltammetry (CV)

A series of SEC experiments were carried out in the reflection cell by means of CV at a fixed concentration of OP 25 mmol L^{-1} and increasing concentrations of Fe(III) in the range 0.01–1.0 mmol L^{-1}. Fig. 3 shows some typical results obtained in this way for three different concentrations of Fe(III): 0.2, 0.5 and 1.0 mmol L^{-1}. The potential scan (Fig. 3a) is the same as in Fig. 2c and the obtained voltammograms present a similar shape. Fig. 3b shows the counts of the 57 spectra registered in every experiment during the evolution of the CV scan. Although the counts at the different wavelengths are practically the same, there is a narrow region around 500 nm where the evolution of the potential produces significant changes in the number of counts. Moreover, the changes become more notorious as the concentration of Fe(III) increases. This strongly suggests that the decrease in the counts is due to the absorption of radiation in the region around 500 nm by the complex of Fe(II) with OP, which is released at the electrode as a consequence of the CV scan. The complex of Fe(III) does not seem to have a significant absorption in this region and, if it was not the case, the calculation of absorbance taking the initial spectrum as a reference would minimise such contribution.

A key point in the treatment of UV–vis spectral data is the signal-to-noise ratio. Working with a low reflectance electrode such as SPCE is more versatile and affordable than using gold screen-printed units. However, the counts achieved are quite lower and this produces a considerable noise which becomes more relevant as the concentration of

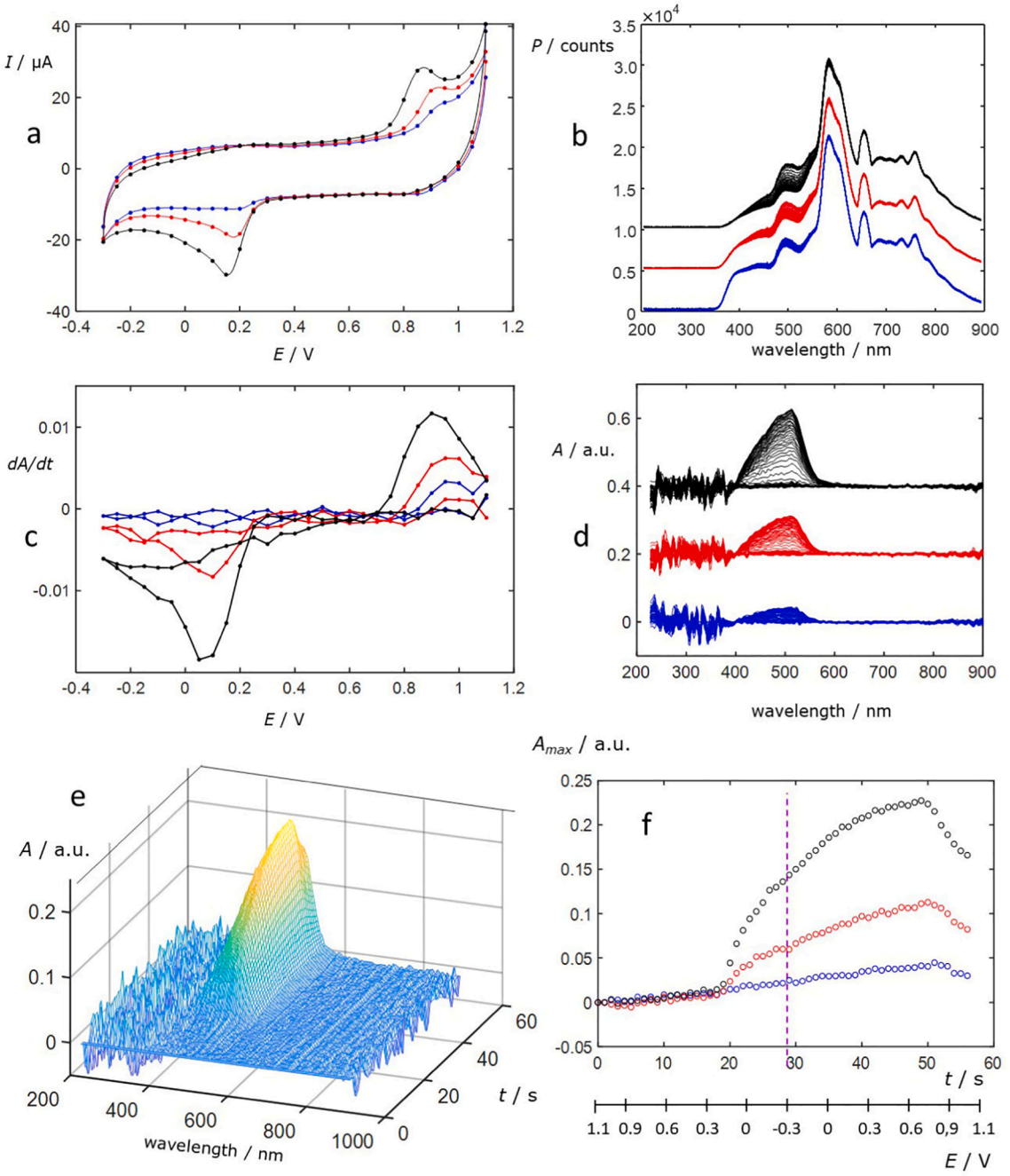

Fig. 3. Typical results of SEC experiments based on CV scans in solutions containing 25 mmol L^{-1} of OP and different concentrations of Fe(III): 0.2 mmol L^{-1} (blue), 0.5 mmol L^{-1} (red) and 1.0 mmol L^{-1} (black). a) CV signals (solid lines) denoting with solid circles the points in which spectra were registered (one spectrum per second); b) radiation power measured by the detector, in counts, as a function of the wavelength; d) absorbance spectra, obtained by dividing every spectra in counts by the first spectrum, just before SEC measurement; c) derivative of the maximum absorbance with respect to the time (solid circles, connected by straight lines); e) 3D plot of absorbance versus wavelength and time for the solution 1.0 mmol L^{-1} Fe(III) and 25 mmol L^{-1} OP; f) maximum absorbance versus time and potential (second axis) for the three solutions above, with a dashed purple line separating forward and backward scans. In figures b and d, red and black spectra have been shifted along the y axis for comparison purposes.

Fe(III) decreases. The application of a DWT to the raw spectra in counts can be a very useful strategy covering two main objectives: compressing the data with minimal loss of information and reducing noise. In this work we have applied DWT using the function 'Daubechies 4′ with 4 compression levels. Fig. S2 shows the results of such transformation on the raw spectrum obtained for the solution containing 0.02 mmol L^{-1} of Fe(III): from the initial 2007 points, the data are compressed into 258 points, which reproduce very well the original spectrum and the noise is notoriously reduced, as shown by the inset in the region where the complex of Fe(II) adsorbs.

Using these compressed and denoised spectra, still in counts, it is possible to obtain reasonable absorbance plots dividing the successive spectra measured in every SEC experiment by the first one (that acquired just before the CV scan). Fig. 3d compares the absorbance spectra obtained for the three concentrations of Fe(III) considered, showing a maximum in the absorbance at *ca.* 510 nm whose height increases with the concentration of Fe(III). It is important to notice the relatively high level of noise registered in the UV region, where counts are scarce. Anyway, this noise is much lower than that obtained when absorbance is computed from raw, not compressed spectra in counts (not shown).

Moreover, the level of noise is comparable at the different concentrations of Fe(III) and, as a consequence, the signal-to-noise ratio increases as the Fe(III) concentration grows and the absorbance peaks go higher (Fig. 3d). Fig. 3e and 3f show a more detailed picture of the evolution of the absorbance spectra along the CV scan as a function of the variable time. In both 3D and 2D plots it is clear that the absorbance only starts to grow when the forward scan approaches potentials sufficiently negative to reduce the Fe(III)-OP complex and the growing continues until the backward scan approaches potentials positive enough to reoxidise it. In good agreement with Eqn. (12), the derivative with respect to the time of the absorbance achieved at 510 nm (Fig. 3f) generates a curve (Fig. 3c) with a similar shape as the CV plot (Fig. 3a). Besides the higher dispersion of optical data, it is interesting to notice the absence of the capacitive contribution which appears in the middle of CV curves (capacitive currents have no optical effects).

Some experiments were made applying a negative deposition potential to accumulate the reduced complex at the electrode surface prior to the CV scan, but no significant improvement of the SEC signals was noticed. This can be due to several reasons: the inefficient mass transport towards the electrode, just by diffusion, the possible electrostatic repulsion at positive potentials between the electrode and the positively charged complex, and the fact that the optical measurements detect the coloured complex not only at the electrode surface, but at any distance inside the optical path. Indeed, deposition at the electrode only shifts the distribution of reagents and products from the bulk to the electrode surface and the diffusion layer. Only species that are being produced or consumed at the electrode are able to change the absorbance, independently of the place where they remain, on the electrode surface or in the solution.

4.3. SEC study by means of chronoamperometry (CA)

A set of chronoamperometric (CA) measurements was carried out at a fixed potential of −0.4 V which, according to the CV plots of Figs. 2 and 3, should provide a potential sufficiently negative to leave the reduction process of the complex of Fe(III) controlled by diffusion. Then, under these conditions and for a planar working electrode such as that of SPCE, the Cottrell expression of Eqn. (2) should hold.

CA measurements were made at the same concentrations of OP and Fe(III) used in the CV study summarised in Fig. 3, and similar SEC effects were detected along the raw spectra in counts (not shown). Nevertheless, a better signal-to-noise ratio was achieved, which allowed us to obtain reasonable data at lower concentrations of Fe(III) than in the case of CV. Fig. 4 shows some examples of the signals obtained in this CA study. It is remarkable, on one hand, the higher difference between the absorbance evolution at different concentrations (Fig. 4d) as compared to the small variations found in the current evolution (Fig. 4a), and, on the other hand, the better signal-to-noise ratio of CA absorbance spectra (Fig. 4c) as compared to these obtained by CV (Fig. 3d).

Fig. 5 deals with possible linearisations, using Cottrell Equation in (2) for electrochemical data (Fig. 5a) and Eqn. (9) for absorbance data (Fig. 5b). In the first case, linear dependence with $t^{-1/2}$ is achieved relatively late, when the current has decreased in a significant way and sensitivity is low. On the contrary, in the second case, a perfect linearity with $t^{1/2}$ is achieved very early and the absorbance is continuously growing with time. This means that, as time goes by, the current is decreasing forced by the low efficiency of mass transport whereas the absorbance is increasing due to the accumulation of the absorbed reduced complex in the diffusion layer. Table S1 summarises the main characteristics of the straight lines fitted to both chronoamperometric and chronoabsorptometric plots. Especially interesting is the study of

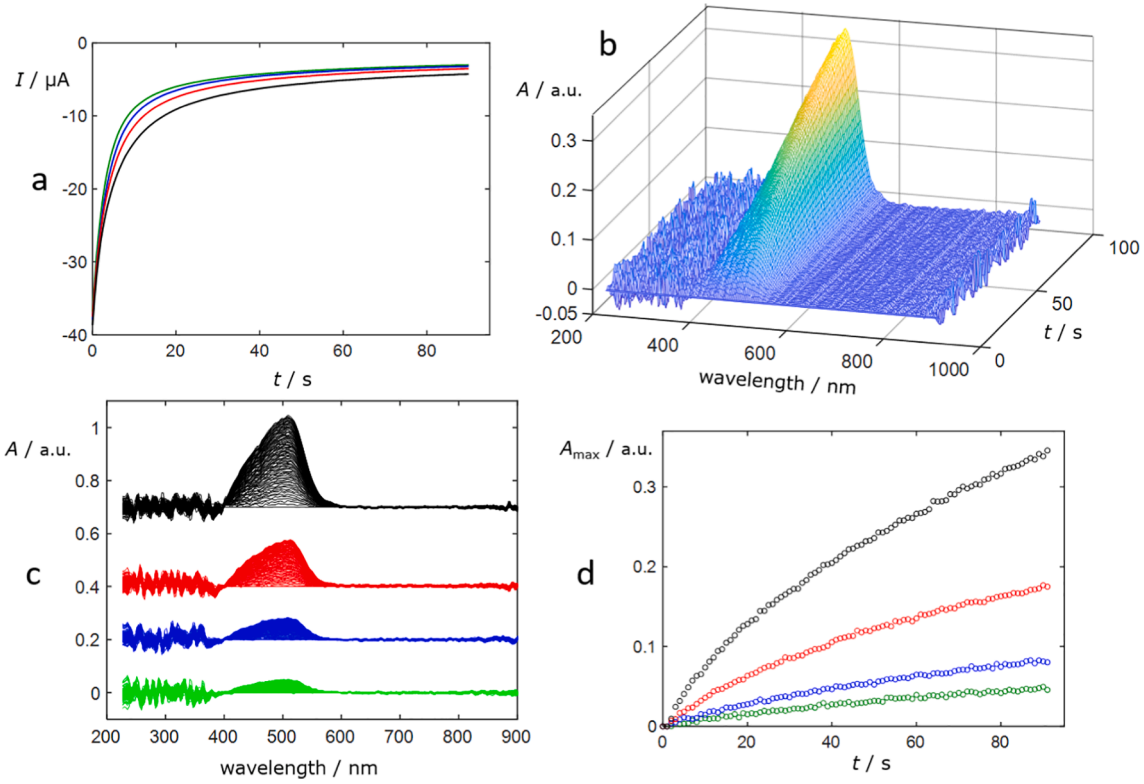

Fig. 4. Typical results of SEC experiments based on chronoamperometric (CA) scans carried out in solutions containing 25 mmol L^{-1} of OP and different concentrations of Fe(III): 0.1 mmol L^{-1} (green), 0.2 mmol L^{-1} (blue), 0.5 mmol L^{-1} (red) and 1.0 mmol L^{-1} (black). a) Currents as a function of time measured when a fixed potential of −0.4 V is applied while one UV–vis spectrum per second is registered; b) Absorbance measured as a function of wavelength and time in the CA experiment carried out for a concentration of 1.0 mmol L^{-1} of Fe(III); c) Absorbance spectra obtained at the different concentrations above; d) Maximum absorbance with respect to the time. In figure c some spectra have been shifted along the y axis for a better comparison of the four data sets.

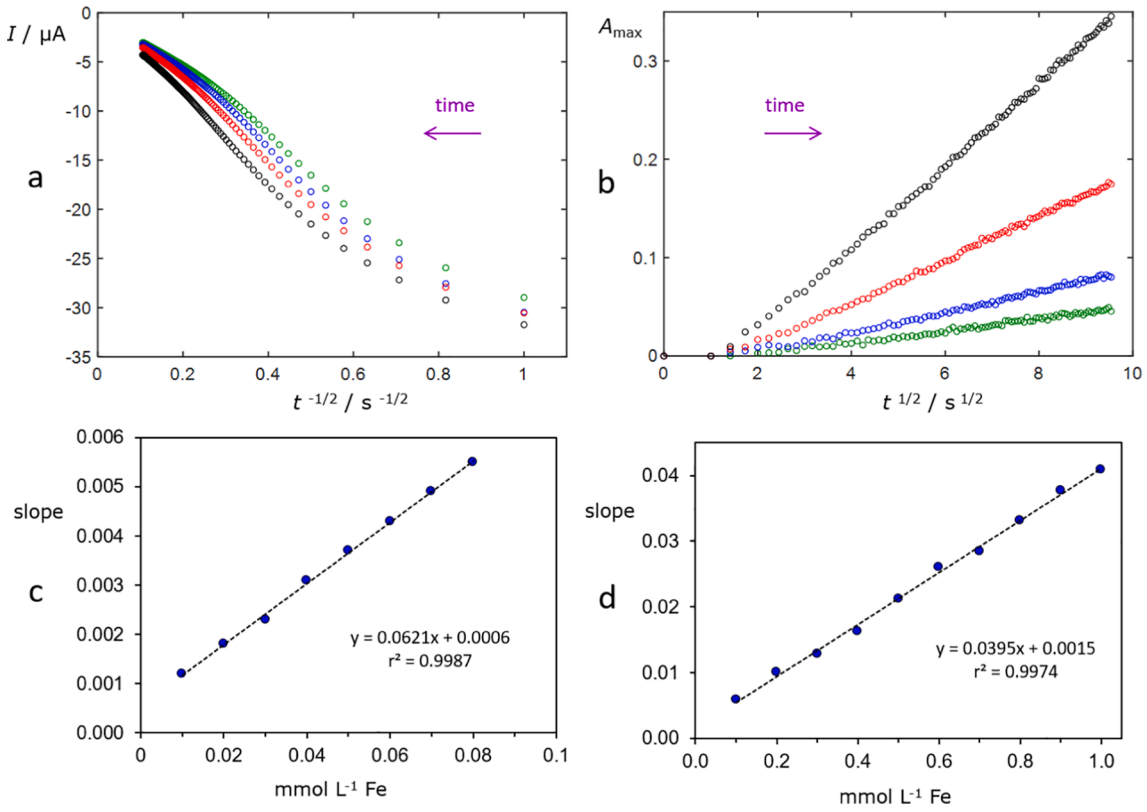

Fig. 5. Linearisation of SEC data using CA scans for a OP concentration 25 mmol L^{-1} and concentrations of Fe(III) 0.1 mmol L^{-1} (green), 0.2 mmol L^{-1} (blue), 0.5 mmol L^{-1} (red) and 1.0 mmol L^{-1} (black): a) Current as a function of $t^{-1/2}$; b) Maximum absorbance as a function of $t^{1/2}$; c) and d) Slopes of the Amax *vs.* $t^{1/2}$ plots as a function of the concentration of Fe(III) inside two different linearity ranges. Purple arrows indicate the evolution of time in the experiments. In c and d the equations and the r^2 coefficients of the calibration lines are indicated inside the plots.

the slopes calculated from Fig. 5a and 5b. Results obtained from currents are linear even at relatively low concentrations of Fe(III). However, slopes only become concentration-dependent at more than 0.10 mmol L^{-1} of Fe(III). In contrast, slopes computed from absorbances are perfectly linear with respect to the concentration of Fe(III), inside two concentration ranges, shown in Fig. 5c and 5d.

At this point, it must be noted the key denoising role of the DWT applied to compress optical data. This is already suggested by the inset of Fig. S2, where the compressed spectrum in counts is quite smoothed as compared to the raw spectrum. Such impression is confirmed when absorbance spectra are computed from the measured counts. Fig. 6 and Table 1 compare the linear plots of the maximum absorbance as a function of $t^{1/2}$ at different concentrations of Fe(III) when absorbance is computed from raw data or from DWT-compressed data. It is clear that compressed data are substantially less noisy and provide more precise slope values than in the case of raw data. Moreover, the differences are more evident as the concentration of Fe(III) decreases.

Table 2 compares some relevant calibration parameters obtained using different strategies in SEC experiments. In the case of CV measurements, the anodic peak measured in the backward scan is much more reliable for calibration than the cathodic scan, notoriously affected by reduction signals of OP. As for chronoamperometric (CA) measurements, the use of Cottrell Equation to carry out calibration from currents is not especially precise (LOD is quite higher than using the anodic CV peak). In contrast, absorbance data acquired along CA measurements provide quite better results, with detection limits at the level of μmol L^{-1}. This can be due, on one hand, to the progressive increase of the concentration of the absorbing species with time and, on the other hand, to the denoising effect of DWT. This is especially true for the use of A_{max} *vs.* $t^{1/2}$ slopes, where the additional denoising effect of the second regression (getting a 'slope of slopes') can play a key role.

Finally, Eqns. (16)–(19) have been applied to the estimation of the diffusion coefficient of the complex Fe(III)-OP. First, chronoamperometric experiments were carried out with potassium ferricyanide and Eqn. (18) was used to estimate the f_R roughness factor by using the diffusion coefficient of ferricyanide, 7.26 10^{-6} cm^2s^{-1}, determined in [25]. A f_R value of 1.15 was found, suggesting that the roughness of SPCE is not especially high (the effective surface was only 15% higher than the geometrical one). With this f_R value, Eqns. (18) and (19) were applied to chronoamperometric and chronoabsorptometric data acquired in solutions containing Fe(III) in the range 0.1–0.9 mmol L^{-1} and OP 25 mol L^{-1} and diffusion coefficients of 7.67 10^{-6} cm^2s^{-1} and 7.73 10^{-6} cm^2s^{-1} were obtained, respectively, for the Fe(III)-OP complex. Both estimates are very similar to each other and also to that of ferricyanide complex, which suggests a good reliablility of chronoabsorptometric data for the estimation of diffusion coefficients of spectroelectrochemically active substances.

4.4. *Chronoamperometric study in the presence of Cu(II)-ion*

In order to evaluate the effect of electrochemical interferences on the performance of the studied methodologies, several experiments were carried out for the Fe(III)-OP system under the same conditions of the previous section but in the presence of 0.1 mmol L^{-1} of Cu(II)-ion.

As Fig. 7 shows, the CV signals measured under these conditions still present the same cathodic and anodic peaks of Fe(III) but with two new overimposed signals, corresponding to the reversible reduction and reoxidation of Cu(II) species. The sensitive overlapping between the reduction signals of Cu(II) and Fe(III) hinders the use of this peak for the determination of Fe(III). However, the presence of copper not only affects this signal, but also the LOD values, which seem to be raised as shown in Table 2. Yet, the strategies based on the measurements of

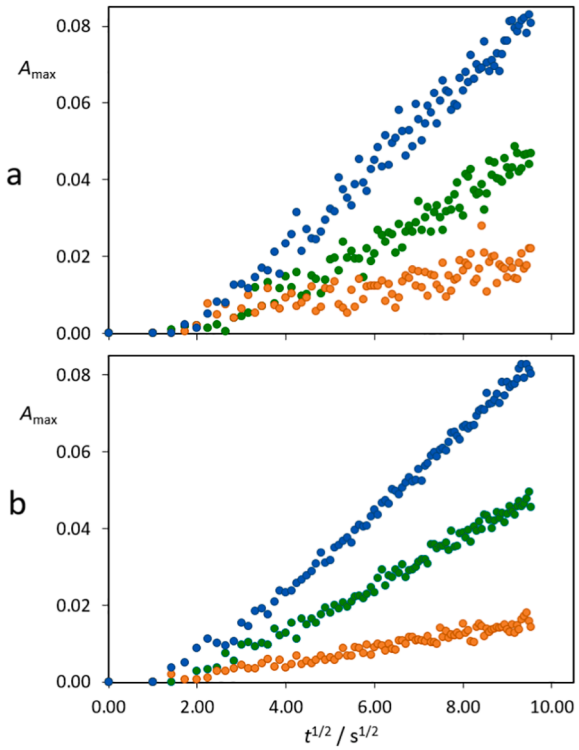

Fig. 6. Effect of DWT on the noise of chronoabsorptiometric data measured for a OP concentration of 25 mmol L^{-1} and Fe(III) concentrations of 0.02 mmol L^{-1} (orange), 0.1 mmol L^{-1} (green) and 0.2 mmol L^{-1} (blue). Results in **a** were obtained from the raw spectra measured at 2007 wavelengths, whereas results in **b** were achieved from the compressed spectra resulting from DWT.

absorbance along CA experiments are much less affected by the interference of Cu(II)-ions, surely due to the increased selectivity provided by the combination of selective potentials and selective wavelengths. Indeed, the slope of the calibration plot in the presence of Cu(II) is 0.061 μA $s^{-1/2}$ mol^{-1} L, very close to that of 0.062 μA $s^{-1/2}$ mol^{-1} L obtained in the absence of Cu(II).

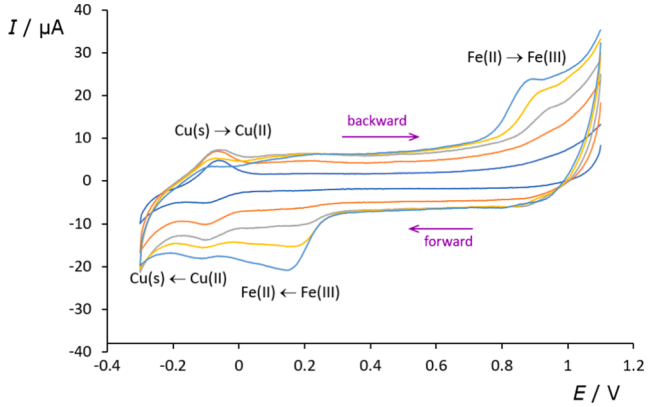

Fig. 7. CV scans registered for a solution containing 25 mmol L^{-1} of OP, 0.1 mmol L^{-1} of Cu(II) and increasing concentrations of Fe(III) (0.02, 0.05, 0.2, 0.5 and 0.8 mmol L^{-1}).

5. Conclusions

From the facts described so far, we can draw the following conclusions:

- SEC in reflection mode can be useful for quantitative analysis, especially when it is based on potential-step chronoamperometry. Indeed, in this case, it would be more appropriate to talk about chronoabsorptometry.
- Chromogenic reagents can enhance the absorption of electrochemically generated substances, as it happens with OP for Fe(II)-ions. This could open a new research line on the application to SEC of traditional chromogenic reagents for metal ions and other inorganic species. In some traditional spectrophotometric methods, the preliminary oxidation or reduction of the analyte could be substituted by its electrochemical generation.
- In reflection mode, accumulation of substances such as Fe(II) or Fe (III) at the electrode surface has no effect on the sensitivity of optical measurements: absorbance detects the analyte at any distance from the electrode and accumulation only moves it from the bulk solution to the electrode surface.
- Among the different possibilities of data treatment, the linearisation of A_{max} *vs.* $t^{1/2}$ yields the best results and the plot of the slopes of the

Table 1
Comparison of the slopes, their relative standard deviations and the r^2 coefficients obtained from chronoabsorptiometric data (A_{max} *vs.* $t^{1/2}$) at three concentrations of Fe(III) using the raw spectra and the spectra compressed by DWT. Linear regression was carried out with points at times higher than 4 s.

$c_{Fe(III)}$ (mmol L^{-1})	slope (mmol^{-1} L $t^{-1/2}$)		RSD slope (%)		r^2	
	raw spectra	compressed spectra	raw spectra	compressed spectra	raw spectra	compressed spectra
0.02	1.92 10^{-3}	1.89 10^{-3}	8.02	3.04	0.6437	0.9265
0.10	6.22 10^{-3}	6.15 10^{-3}	2.54	1.27	0.9474	0.9864
0.20	1.08 10^{-2}	1.04 10^{-2}	1.57	0.84	0.9793	0.9940

Table 2
Calibration parameters resulting from data acquired from SEC experiments in different ways. Linear ranges are computed from LOQ to the end of linearity.

Type of data	Fe(III) alone			Fe(III) + 0.1 mmol L^{-1} Cu(II)		
	linear range (mmol L^{-1})	r^2	LOD (mmol L^{-1})	linear range (mmol L^{-1})	r^2	LOD (mmol L^{-1})
CV current (cathodic peak)	0.17 – 1.00	0.9851	0.052	–	–	–
CV current (anodic peak)	0.04 – 1.00	0.9992	0.012	0.2 – 1.0	0.9835	0.064
CA current *I vs.* $t^{-1/2}$	0.12 – 0.90	0.9967	0.037	0.6 – 1.0	0.9358	0.194
CA A_{max}	0.02 – 0.08	0.9896	0.006	0.06 – 0.09	0.9395	0.018
	0.10 – 1.00	0.9977	-	0.10 – 1.00	0.9649	-
CA slope A_{max} *vs.* $t^{1/2}$	0.007 – 0.08	0.9987	0.002	0.02 – 0.09	0.9890	0.007
	0.10 – 1.00	0.9974	-	0.10 – 1.00	0.9574	-

lines as a function of the concentration of Fe(III) provides a sensitive and reliable strategy for quantification with detection limits in the μmol L^{-1} range. The application of discrete wavelet transform to raw spectral data and the fitting of regression lines are very relevant for improving the signal-to-noise ratio and, thus, achieving detection limits comparable to these attained with SEC in parallel configuration.

- The linear relationship between A_{max} and $t^{1/2}$ in chronoabsorptometric experiments can be used to estimate diffusion coefficients from molar absorptivities and vice-versa.
- The experiments in the presence of Cu(II)-ions suggest that the proposed methodology could be quite unaffected by the presence of other electroactive substances. This is due to the enhanced selectivity of SEC when the separate selectivities of amperometry (related to potential) and absorptometry (related to wavelength) are combined.

Thus, it seems that not only parallel configurations and long path-length cells are suitable for quantification using SEC equipment. The present work shows that normal configuration and reflection cells offer interesting possibilities for analytical applications that should be investigated.

CRediT authorship contribution statement

G. Sirin Ustabasi: Methodology, Formal analysis, Investigation, Writing – review & editing, Visualization. **Julio Bastos-Arrieta:** Conceptualization, Methodology, Formal analysis, Writing – review & editing, Visualization, Supervision, Resources. **Clara Pérez-Ràfols:** Conceptualization, Methodology, Formal analysis, Writing – review & editing, Visualization, Supervision, Resources. **Núria Serrano:** Conceptualization, Methodology, Formal analysis, Writing – review & editing, Visualization, Supervision, Resources. **José Manuel Díaz-Cruz:** Conceptualization, Methodology, Formal analysis, Validation, Writing – original draft, Visualization, Supervision, Resources.

Declaration of Competing Interest

The authors declare the following financial interests/personal relationships which may be considered as potential competing interests.

Acknowledgments

This work is supported by the Ministry of Science and Innovation of Spain (Project PID2019-107102RB-C22).

Gul Sirin Ustabasi acknowledges the grant provided to her by the Scientific and Technological Research Council of Turkey (TUBITAK) in the frame of 2214-A International Research Fellowship Programme for PhD Students.

Authors are especially grateful to Aránzazu Heras and Álvaro Colina, from the University of Burgos, for their valuable advices and kind assistance in both theoretical and experimental aspects of spectroelectrochemistry using reflection cells.

J.M. Diaz Cruz reports financial support was provided by Spain Ministry of Science and Innovation.

Appendix A. Supplementary data

Supplementary data to this article can be found online at https://doi.org/10.1016/j.microc.2022.107678.

References

[1] W.R. Heineman, Spectroelectrochemistry: the combination of optical and electrochemical techniques, J. Chem. Educ. 60 (1983) 305, https://doi.org/10.1021/ed060p305.
[2] D.A. Scherson, Y.V. Tolmachev, I.C. Stefan, Ultraviolet/visible spectroelectrochemistry, in: R.A. Meyers (Ed.), Encyclopedia of Analytical Chemistry: Applications, Theory and Instrumentation, John Wiley, Chichester, 2000.
[3] A.J. Bard, L.R. Faulkner, Electrochemical Methods: Fundamentals and Applications, Chapter 17: Spectroelectrochemistry and other coupled characterization methods, 2nd Edn, John Wiley, New York, 2001.
[4] W. Kaim, J. Fiedler, Spectroelectrochemistry: the best of two worlds, Chem. Soc. Rev. 38 (2009) 3373–3382, https://doi.org/10.1039/B504286K.
[5] T. Kuwana, R.K. Darlington, D.W. Leedy, Electrochemical studies using conducting glass indicator electrodes, Anal. Chem. 36 (1964) 2023–2025, https://doi.org/10.1021/ac60216a003.
[6] J. Garoz-Ruiz, J.V. Perales-Rondon, A. Heras, A. Colina, Spectroelectrochemical sensing: current trends and challenges, Electroanalysis 31 (2019) 1254–1278, https://doi.org/10.1002/elan.201900075.
[7] J.B. He, Y. Wang, N. Deng, X.Q. Lin, Study of the adsorption and oxidation of antioxidant rutin by cyclic voltammetry–voltabsorptometry, Bioelectrochemistry 71 (2007) 157–163, https://doi.org/10.1016/j.bioelechem.2007.03.003.
[8] P. Shi, I. Fromondi, Q. Shi, Z. Wang, D.A. Scherson, Simultaneous in situ reflectance and probe beam deflection measurements at solid electrode– aqueous electrolyte interfaces, Anal. Chem. 79 (2007) 202–207, https://doi.org/10.1021/ac061452i.
[9] V. Ruiz, A. Colina, M.Á. Heras, J. López-Palacios, Quantized spectroelectrochemical behaviour of monolayer-protected gold cluster films assessed by reflectance spectroelectrochemical quartz crystal microbalance, Electrochem. Commun. 9 (2007) 255–261, https://doi.org/10.1016/j.elecom.2006.09.019.
[10] E. Tesařová, A. Heras, A. Colina, V. Ruiz, I. Švancara, K. Vytřas, J. López-Palacios, A spectroelectrochemical approach to the electrodeposition of bismuth film electrodes and their use in stripping analysis, Anal. Chim. Acta 608 (2008) 140–146, https://doi.org/10.1016/j.aca.2007.12.023.
[11] K.C. Honeychurch, J.P. Hart, Screen-printed electrochemical sensors for monitoring metal pollutants, Trends Anal. Chem. 22 (2003) 456–469, https://doi.org/10.1016/S0165-9936(03)00703-9.
[12] J. Barton, M.B.G. García, D.H. Santos, P. Fanjul-Bolado, A. Ribotti, M. McCaul, D. Diamond, P. Magni, Screen-printed electrodes for environmental monitoring of heavy metal ions: a review, Microchim. Acta 183 (2016) 503–517, https://doi.org/10.1007/s00604-015-1651-0.
[13] P. Yáñez-Sedeño, S. Campuzano, J.M. Pingarrón, Screen-printed electrodes: promising paper and wearable transducers for (bio) sensing, Biosensors 10 (2020) 76, https://doi.org/10.3390/bios10070076.
[14] E. Costa-Rama, M.T. Fernández-Abedul, Paper-based screen-printed electrodes: a new generation of low-cost electroanalytical platforms, Biosensors 11 (2021) 51, https://doi.org/10.3390/bios11020051.
[15] N. González-Diéguez, A. Colina, J. López-Palacios, A. Heras, Spectroelectrochemistry at screen-printed electrodes: Determination of dopamine, Anal. Chem. 84 (2012) 9146–9153, https://doi.org/10.1021/ac3018444.
[16] J. Garoz-Ruiz, A. Heras, A. Colina, Direct determination of ascorbic acid in a grapefruit: paving the way for in vivo spectroelectrochemistry, Anal. Chem. 89 (2017) 1815–1822, https://doi.org/10.1021/acs.analchem.6b04155.
[17] J. Garoz-Ruiz, C. Guillen-Posteguillo, A. Heras, A. Colina, Simplifying the assessment of parameters of electron-transfer reactions by using easy-to-use thin-layer spectroelectrochemistry devices, Electrochem. Commun. 86 (2018) 12–16, https://doi.org/10.1016/j.elecom.2017.11.001.
[18] J. Garoz-Ruiz, C. Guillen-Posteguillo, A. Colina, A. Heras, Application of spectroelectroanalysis for the quantitative determination of mixtures of compounds with highly overlapping signals, Talanta 195 (2019) 815–821, https://doi.org/10.1016/j.talanta.2018.12.002.
[19] F. Olmo, A. Rodriguez, A. Colina, A. Heras, UV/Vis absorption spectroelectrochemistry of folic acid, J. Solid State Electrochem. 26 (2022) 29–37, https://doi.org/10.1007/s10008-021-05026-5.
[20] A. Martell, R.M. Smith, Critical Stability Constants, Plenum press, New York, 1974.
[21] G.L. Smith, A.A. Reutovich, A.K. Srivastava, R.E. Reichard, C.H. Welsh, A. Melman, F. Bou-Abdallah, Complexation of ferrous ions by ferrozine, 2, 2′-bipyridine and 1, 10-phenanthroline: Implication for the quantification of iron in biological systems, J. Inorg. Biochem. 220 (2021), 111460, https://doi.org/10.1016/j.jinorgbio.2021.111460.
[22] G.S. Ustabasi, C. Pérez-Ràfols, N. Serrano, J.M. Díaz-Cruz, Simultaneous determination of iron and copper using screen-printed carbon electrodes by adsorptive stripping voltammetry with o-phenanthroline, Microchem. J. 179 (2022), 107597, https://doi.org/10.1016/j.microc.2022.107597.
[23] C. Pérez-Ràfols, N. Serrano, J.M. Díaz-Cruz, A hybrid sensing system combining simultaneous optical and electrochemical measurements: Application to beer discrimination, Talanta 241 (2022), 123273, https://doi.org/10.1016/j.talanta.2022.123273.
[24] Matlab, Version R2021b Ed., Mathworks Inc., Natick, MA, USA, 2021.
[25] S.J. Konopka, B. McDuffie, Diffusion coefficients of ferri-and ferrocyanide ions in aqueous media, using twin-electrode thin-layer electrochemistry, Anal. Chem. 42 (14) (1970) 1741–1746.